BIOLOGICAL CRYSTALLOGRAPHY

ISSN 1399-0047

Structural evidence for asymmetric ligand binding to transthyretin

Michele Cianci,[a] Claudia Folli,[b] Francesco Zonta,[c] Paola Florio,[d] Rodolfo Berni[d]* and Giuseppe Zanotti[e]*

[a]EMBL Hamburg Outstation, c/o DESY, Building 25a, Notkestrasse 85, 22603 Hamburg, Germany, [b]Department of Food Science, University of Parma, Viale G. Usberti 23/a, 43124 Parma, Italy, [c]Shangai Institute for Advanced Immunochemical Studies (SIAIS), ShanghaiTech University, No. 99 Haike Road, Pudong, Shanghai 201210, People's Republic of China, [d]Department of Life Sciences, University of Parma, Viale G. Usberti 23/a, 43124 Parma, Italy, and [e]Department of Biomedical Sciences, University of Padua, Viale G. Colombo 3, 35131 Padova , Italy. *Correspondence e-mail: rodolfo.berni@unipr.it, giuseppe.zanotti@unipd.it

Received 29 October 2014
Accepted 1 June 2015

Edited by M. Schiltz, Fonds National de la Recherche, Luxembourg

Keywords: transthyretin; amyloidosis; protein misfolding; negative cooperativity; fibrillogenesis inhibitors; transthyretin stabilizers.

PDB references: TTR–apigenin complex, 4wo0; TTR–pterostilbene complex, 4wns; TTR–quercetin complex, 4wnj

Supporting information: this article has supporting information at journals.iucr.org/d

Human transthyretin (TTR) represents a notable example of an amyloidogenic protein, and several compounds that are able to stabilize its native state have been proposed as effective drugs in the therapy of TTR amyloidosis. The two thyroxine (T4) binding sites present in the TTR tetramer display negative binding cooperativity. Here, structures of TTR in complex with three natural polyphenols (pterostilbene, quercetin and apigenin) have been determined, in which this asymmetry manifests itself as the presence of a main binding site with clear ligand occupancy and related electron density and a second minor site with a much lower ligand occupancy. The results of an analysis of the structural differences between the two binding sites are consistent with such a binding asymmetry. The different ability of TTR ligands to saturate the two T4 binding sites of the tetrameric protein can be ascribed to the different affinity of ligands for the weaker binding site. In comparison, the high-affinity ligand tafamidis, co-crystallized under the same experimental conditions, was able to fully saturate the two T4 binding sites. This asymmetry is characterized by the presence of small but significant differences in the conformation of the cavity of the two binding sites. Molecular-dynamics simulations suggest the presence of even larger differences in solution. Competition binding assays carried out in solution revealed the presence of a preferential binding site in TTR for the polyphenols pterostilbene and quercetin that was different from the preferential binding site for T4. The TTR binding asymmetry could possibly be exploited for the therapy of TTR amyloidosis by using a cocktail of two drugs, each of which exhibits preferential binding for a distinct binding site, thus favouring saturation of the tetrameric protein and consequently its stabilization.

1. Introduction

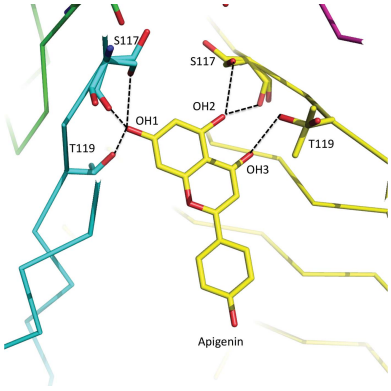

Transthyretin (TTR) is an oligomeric protein formed by the association of four chemically identical subunits, each of about 13.5 kDa, and its structure is known at high resolution (Blake *et al.*, 1978; Hörnberg *et al.*, 2000). TTR is involved in the transport of thyroxine (T4) in extracellular fluids and in the co-transport of vitamin A by forming a macromolecular complex with plasma retinol-binding protein (RBP4) (Monaco *et al.*, 1995; Wojtczak *et al.*, 1996). The TTR monomer is composed of two four-stranded antiparallel β-sheets and a short α-helix. Two monomers are held together to form a stable dimer through a network of hydrogen-bond interactions involving the two edge β-strands H and F of each monomer in such a way that a pseudo-continuous eight-stranded β-sandwich is generated. Finally, two dimers

Table 1
Data-collection and refinement statistics.

Data were measured on the PXIII beamline at the Synchrotron Light Source, Villigen, Switzerland. Values in parentheses are for the last resolution shell.

Data set	TTR–quercetin	TTR–pterostilbene	TTR–apigenin	TTR–tafamidis
Wavelength	1.00	1.00	1.00	1.00
Unit-cell parameters				
a (Å)	42.86	42.70	42.66	42.46
b (Å)	85.78	85.58	85.74	85.24
c (Å)	63.87	64.15	63.98	63.11
Resolution (Å)	42.89–1.40 (1.47–1.40)	42.79–1.40 (1.47–1.40)	42.87–1.34 (1.41–1.34)	42.62–1.46 (1.54–1.46)
$R_{\rm merge}$†	0.032 (0.481)	0.026 (0.536)	0.031 (0.465)	0.047 (0.691)
$R_{\rm p.i.m.}$‡	0.020 (0.319)	0.014 (0.291)	0.016 (0.336)	0.026 (0.382)
$\langle I/\sigma(I)\rangle$	27.3 (3.4)	36.9 (3.8)	26.2 (2.8)	19.8 (2.5)
Completeness (%)	99.6 (98.5)	99.8 (99.0)	98.3 (94.5)	98.9 (97.9)
Multiplicity	6.3 (6.0)	6.4 (6.1)	5.7 (3.8)	5.5 (5.1)
Refinement				
No. of reflections	47208	47156	52413	40373
$R_{\rm work}/R_{\rm free}$	0.157/0.193	0.168/0.185	0.186/0.206	0.182/0.230
No. of atoms				
Total	2046	2064	2142	1952
Protein	1811	1840	1813	1803
Solvent	205	183	289	209
Ligands	30	41	40	40
R.m.s. deviations				
Bond lengths (Å)	0.013	0.010	0.006	0.009
Bond angles (°)	1.44	1.31	1.08	1.28
Ramachandran plot§ (%)				
Favoured	97.84	97.45	98.70	97.80
Allowed	2.16	2.55	1.30	2.20
Outliers	0	0	0	0
Rotamer outliers§ (%)	1.02	0.99	0.00	1.0
C^{β} deviations§	0	0	0	0

† $R_{\rm merge} = \sum_{hkl}\sum_i |I_i(hkl) - \langle I(hkl)\rangle| / \sum_{hkl}\sum_i I_i(hkl)$, where $I_i(hkl)$ is the intensity of a reflection and $\langle I(hkl)\rangle$ is the mean intensity of all symmetry-related reflections *hkl*. ‡ $R_{\rm p.i.m.} = \sum_{hkl}\{1/[N(hkl)-1]\}^{1/2}\sum_i |I_i(hkl) - \langle I(hkl)\rangle| / \sum_{hkl}\sum_i I_i(hkl)$, where $I_i(hkl)$ is the intensity of a reflection, $\langle I(hkl)\rangle$ is the mean intensity of all symmetry-related reflections *hkl* and $N(hkl)$ is the multiplicity (Weiss, 2001). § *MolProbity* statistics.

associate back to back, mainly through a few hydrophobic contacts between residues of the AB and GH loops, to form the tetramer, in which a central cavity harbouring two T4 binding sites traverses the entire tetramer.

TTR is associated with human diseases. In fact, it is one of more than 30 amyloidogenic human proteins that can lead to the extracellular accumulation in tissues of cross-β-sheet amyloid fibrils, which are responsible for degenerative diseases known as amyloidoses. In the case of TTR, amyloidoses, which are related to the predominant deposition of fibrillar aggregates in peripheral nerves and in the heart, are mainly represented by a sporadic disease known as senile systemic amyloidosis (SSA), which is caused by wild-type TTR in old age (Westermark *et al.*, 1990), and familial amyloidotic polyneuropathy (FAP) and cardiomyopathy (FAC), which are caused by a large number of amyloidogenic mutations (Johnson *et al.*, 2005; Connelly *et al.*, 2010). Evidence has been obtained to indicate that such mutations enhance the intrinsic amyloidogenic potential of wild-type TTR by destabilizing its native state (Hurshman Babbes *et al.*, 2008; Cendron *et al.*, 2009). A list of amyloidogenic mutations of TTR is available at http://amyloidosismutations.com. Notably, T4 and other specific TTR ligands establish interactions with the pair of subunits whose residues line each hormone-binding cavity in the central channel. As a result, such interactions are able to bridge neighbouring subunits at the dimer–dimer interface, thereby stabilizing the TTR tetramer. X-ray analysis of TTR in complex with a variety of chemically different ligands has become a well established methodology in the last decade for the design of new TTR stabilizers, which are inhibitors of TTR fibrillogenesis (Johnson *et al.*, 2005; Choi *et al.*, 2010; Connelly *et al.*, 2010; Kolstoe & Wood, 2010; Bulawa *et al.*, 2012; Palaninathan, 2012; Zanotti *et al.*, 2013). Among them, tafamidis was found to possess favourable features, such as highly selective binding to TTR in human plasma (Bulawa *et al.*, 2012) and the ability to slow neurological impairment in TTR amyloidosis (Coelho *et al.*, 2013), and has recently been approved by the EMA (European Medicines Agency) for the treatment of TTR FAP (Johnson *et al.*, 2012). Moreover, natural compounds such as polyphenols, both stilbenoids and flavonoids, are able to specifically interact with the T4 binding sites of TTR, leading to protein stabilization and inhibition of fibrillogenesis (Klabunde *et al.*, 2000; Green *et al.*, 2005; Trivella *et al.*, 2010, 2012).

Despite the presence in the TTR tetramer of two identical binding sites, which are both occupied by T4 in the crystal with a roughly similar mode of binding (Wojtczak *et al.*, 1996), the binding of T4 in solution is characterized by a strong negative cooperativity (Ferguson *et al.*, 1975; Cheng *et al.*, 1977). In this respect, it should be noted that previous crystallographic studies with a monoclinic crystal form of TTR at 3 Å resolution revealed that the two T4 ligands are oriented differently in each binding site, with large conformational changes of the side chains present in the cavities (Wojtczak *et al.*, 2001).

In this study, we have analyzed the crystal structures of complexes of TTR with three natural polyphenols, which *in vitro* show discrete binding affinity for TTR. These data, coupled with the results of competition binding experiments in solution and of molecular-dynamics calculations, provide insight into the cooperative behaviour of TTR with regard to its interaction with ligands.

2. Experimental procedures

2.1. Crystal structure determination

Recombinant human wild-type TTR was prepared as described by Pasquato *et al.* (2007). Crystals of ligand–TTR complexes were obtained at room temperature in about one week by co-crystallization using the hanging-drop vapour-

diffusion method. The protein (5 mg ml^{-1}) in 20 m*M* sodium phosphate pH 7 was incubated for a few hours with a fourfold molar excess of ligand solubilized in DMSO, with the exception of pterostilbene, which was solubilized in ethanol. Drops were formed by mixing equal volumes of the solution containing the ligand–TTR complex and the reservoir/precipitant solution (2.0 *M* ammonium sulfate, 0.1 *M* KCl, 0.05 *M* sodium phosphate pH 7.0). The data sets for the different ligand–TTR complexes were collected on the PXIII beamline at the Swiss Light Source synchrotron-radiation facility, Villigen, Switzerland. All crystals belonged to the orthorhombic space group $P2_12_12$, as does the wild-type TTR, with two monomers in the asymmetric unit. Data sets were processed with *XDS* (Kabsch, 2010) and scaled with *SCALA* (Evans, 2006) from the *CCP*4 suite (Winn *et al.*, 2011). The structures of the TTR–ligand complexes were refined starting from the dimer of uncomplexed TTR as a template (PDB entry 1f41; Hörnberg *et al.*, 2000). The models were refined using the *PHENIX* package (Adams *et al.*, 2010). In the last cycles, TLS refinement was applied. Map visualization and manual adjustment of the models were performed using the *Coot* graphical interface (Emsley & Cowtan, 2004). Atomic coordinates of the inhibitor molecules and restraints were obtained from the *PRODRG* server (Painter & Merritt, 2006). Data-collection and refinement statistics are given in Table 1.

2.2. Equilibrium molecular dynamics

From the atomic coordinates of the structure of TTR, a molecular-dynamics model was built using the *GROMACS* 5 package (Pronk *et al.*, 2013), following the procedure used for the simulation of other systems (see, for example, Zonta *et al.*, 2015). After adding H atoms, the model underwent a short energy minimization in vacuum and was then solvated with full-atom TIP3P water containing Cl^- and K^+ ions at a concentration of ∼0.15 *M* in order to mimic a physiological ionic strength. The whole system consisted of 76 969 atoms. We initially performed a short energy-minimization run, followed by equilibrium molecular dynamics under periodic boundary condition using a cubic unit cell whose sides measured 9.22 nm. Equilibrium molecular-dynamics simulations performed using the AMBER03 force field (Duan *et al.*, 2003) under constant NPT conditions lasted more than 170 ns. The temperature T and pressure P were kept constant at 300 K and 101.3 kPa, respectively, using the Berendsen thermostat and barostat (Berendsen *et al.*, 1984). Fast smooth particle–mesh Ewald summation (Darden *et al.*, 1993) was used for long-range electrostatic interactions, with a cutoff of 1.0 nm for direct interactions.

For each atom, the root-mean-square fluctuation (r.m.s.f.) around the average position was computed over the molecular-dynamics trajectory, defined as

$$\text{r.m.s.f.}(i) = \frac{1}{T}[x_i(t) - \overline{x}_i], \qquad (1)$$

where $x_i(t)$ is the position of the ith atom at time t, $\overline{x}_i$ is its average position along the whole trajectory and T is the total time length of the trajectory. R.m.s.f was computed using *g_covar* from the *GROMACS* package (Pronk *et al.*, 2013).

2.3. Calculation of the correlation of distances of corresponding residues

In order to understand the dynamics of the two binding cavities in TTR in detail, the distances between the C^α positions of all pairs of corresponding residues in the AA' and BB' dimers (Δ_1 and Δ_2, respectively) were computed as a function of time. The results for the central residues (112–119) are reported in Fig. 4(*b*). The correlation between the two traces was then computed as

$$\rho(i) = \frac{\sum_{t=0}^{T}[\Delta_1(t) - \overline{\Delta}_1][\Delta_2(t) - \overline{\Delta}_2]}{\left\{\sum_{t=0}^{T}[\Delta_1(t) - \overline{\Delta}_1]^2\right\}^{1/2}\left\{\sum_{t=0}^{T}[\Delta_2(t) - \overline{\Delta}_2]^2\right\}^{1/2}}, \qquad (2)$$

where an overline represents the time average of a quantity. From this definition, ρ is a function of the amino acids in one

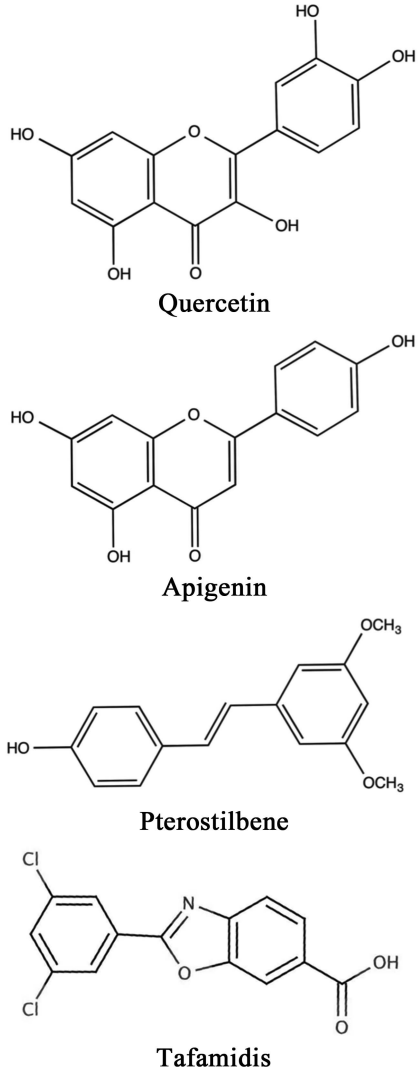

Figure 1
Structural formulae of TTR ligands.

of the monomeric units. The results of the correlations are summarized in Fig. 5(*a*) and in Supplementary Fig. S2.

2.4. Competition binding assays using radiolabelled T4

TTR was incubated with a trace amount of radiolabelled ^{125}I-L-T4 (Perkin Elmer; specific activity of ∼1250 µCi µg^{-1}) in the absence or in the presence of increasing concentrations of pterostilbene or quercetin in PBS buffer for 1 h at room temperature. Samples were then subjected to nondenaturing PAGE and the radioactivity signals were recorded with a Cyclone Storage Phosphor Screen (Packard BioScience).

2.5. Fluorometric competition binding assays

The interaction between TTR and pterostilbene was assessed by exploiting the fluorescence emission of the TTR-bound stilbenoid. TTR was supplemented with increasing concentrations of pterostilbene in the absence or the presence of T4, and fluorescence emission spectra were recorded (excitation at 320 nm). To evaluate the ability of quercetin (a

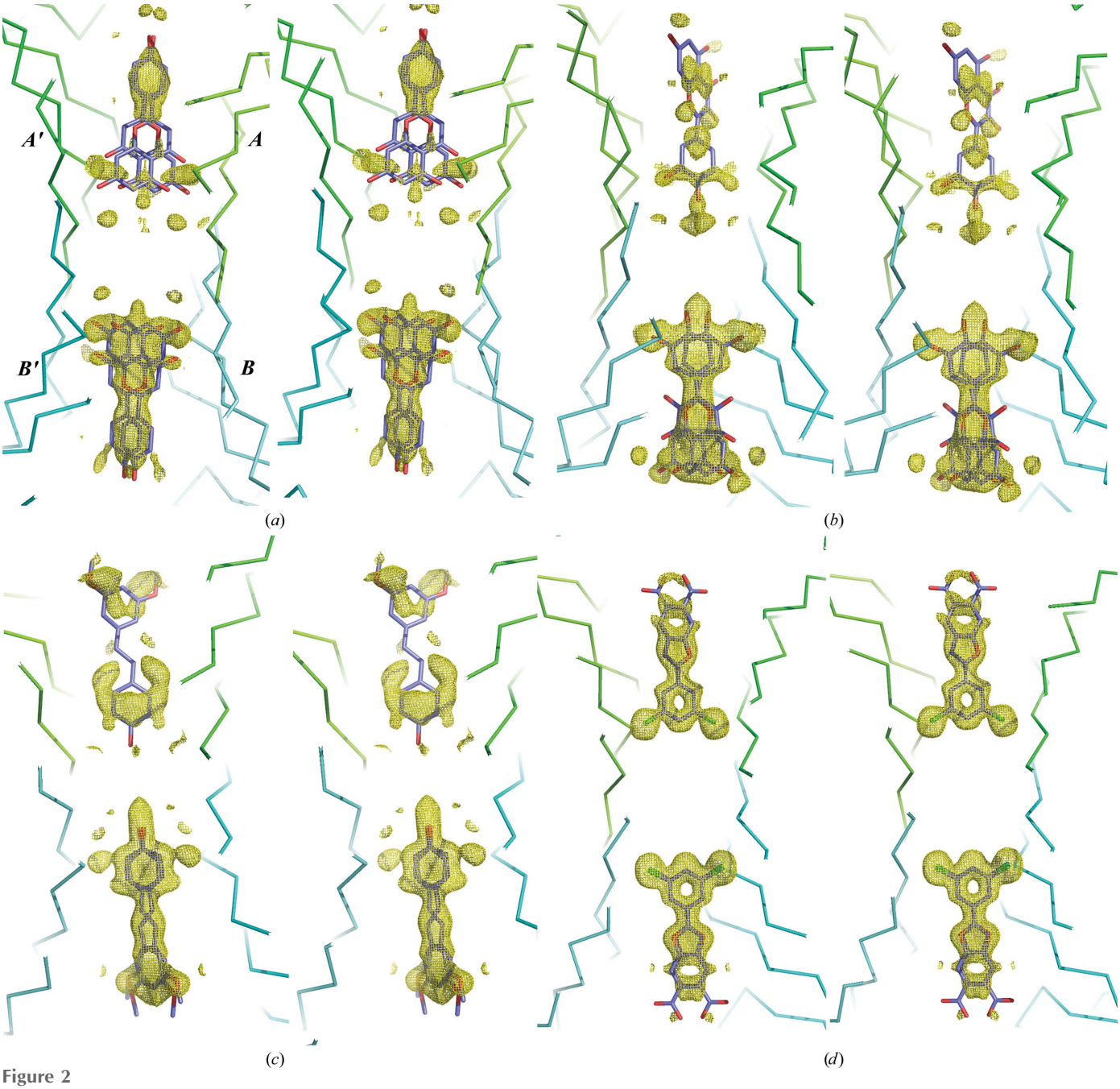

Figure 2
Difference Fourier electron-density maps of the binding cavity of TTR in complex with (*a*) apigenin, (*b*) quercetin, (*c*) pterostilbene and (*d*) tafamidis. Maps were calculated with ($F_{obs} - F_{calc}$) coefficients and calculated phases from the model deprived of the ligand. Maps are contoured at 2.5σ. Partial C$^{\alpha}$ chain traces are shown in two different shades of green and cyan for monomers *A* and *A*′ and for monomers *B* and *B*′, respectively. The ligand-binding sites *A* and *B* are in the upper and lower parts of each panel, respectively.

nonfluorescent ligand) to compete with TTR-bound pterostilbene, similar experiments were conducted by adding quercetin to TTR pre-incubated with pterostilbene. Fluorescence binding experiments were carried out in 50 m*M* sodium phosphate buffer, 150 m*M* sodium chloride pH 7.4 at 25°C using a Perkin Elmer LS-50B spectrofluorometer.

3. Results

3.1. Crystal structures of TTR–ligand complexes

Two of the three TTR-bound polyphenols considered in this study (quercetin and apigenin) belong to the flavonoid family, whilst the third (pterostilbene) is a stilbenoid which is chemically related to resveratrol, another TTR ligand whose interactions with TTR have been characterized structurally in a previous study (PDB entry 1dvs; Klabunde *et al.*, 2000; Fig. 1). Crystals of human TTR in complex with these ligands obtained using a co-crystallization method diffracted to a maximum resolution between 1.34 and 1.40 Å, and this allowed us to define the details of the T4 binding sites and to refine the occupancies of the ligands in the TTR molecule quite carefully. X-ray diffraction data have also been collected for TTR in complex with tafamidis, which is used as a reference high-affinity ligand. As expected, the crystal structures of the TTR–ligand complexes do not show any major differences when compared with that of uncomplexed human TTR (PDB entry 1f41; Hörnberg *et al.*, 2000). The crystal structures of the three TTR–polyphenol complexes are also very similar: the r.m.s.d.s between equivalent C^{α} atoms for each pair are 0.24, 0.24 and 0.24 Å for complexes of TTR with quercetin or pterostilbene, quercetin or apigenin, and pterostilbene or apigenin, respectively. Owing to the relatively high resolution (better than 1.4 Å), several side chains can be observed in double conformations: four in the complexes of TTR with quercetin and apigenin (Ser117 and Thr119 in both chains *A* and *B*) and nine in the TTR–pterostilbene complex (Cys10, Phe24 and Glu66 in chain *A* and Glu72, Ser117 and Thr119 in both chains *A* and *B*). Some molecules of buffer or precipitant are also visible in some cases, but always in regions far from the binding site and thus not interfering with the binding of the ligand.

The central cavity of TTR, in which the T4 hormone or other small ligands can bind, is generated by the interaction between two dimers labelled *AB* and *A*′*B*′. In the TTR crystals belonging to space group $P2_12_12$, only one dimer, *AB*, is present in the asymmetric unit, so that the *A*′*B*′ dimer is identical to the *AB* dimer by crystal symmetry. This implies the presence of two symmetric binding sites, one lined by monomers *A* and *A*′ and the other by monomers *B* and *B*′, labelled the *A* and *B* binding sites, respectively. In the crystal structures of TTR in complex with quercetin, pterostilbene and apigenin, after a few cycles of refinement and before any ligand was fitted, the electron density expected for the ligand was clearly visible in site *B*, whilst the same density in site *A* was much weaker or barely visible. In the case of apigenin, the ligand was fitted in both sites, with occupancies that refined to 0.46 and 0.21 for sites *B* and *A*, respectively (given the symmetry of each site, this corresponds to occupancies of 92 and 42%, respectively), but the electron-density map (Fig. 2*a*) suggests an even lower occupancy for the second site. In the case of the quercetin–TTR and pterostilbene–TTR complexes, a ligand was only fitted in site *B*, since the electron density in site *A* was very weak (Figs. 2*b* and 2*c*).

3.1.1. TTR–apigenin complex. TTR-bound apigenin is mostly oriented with the benzopyran ring inside the cavity and the hydroxyphenyl ring pointing towards the solvent, and only a small amount of it, if any, is bound in the reverse orientation. The latter orientation was instead observed in the previously solved structure of the TTR–apigenin complex (PDB entry 4der; Trivella *et al.*, 2012). We do not know whether this different behaviour can be ascribed to the lower resolution (1.8 Å) for the complex with PDB code 4der or to the different conditions used for the crystallization of the TTR–apigenin complex. In our crystal structure the two hydroxyl groups of the benzopyran ring form hydrogen bonds to the O^{γ} atom of

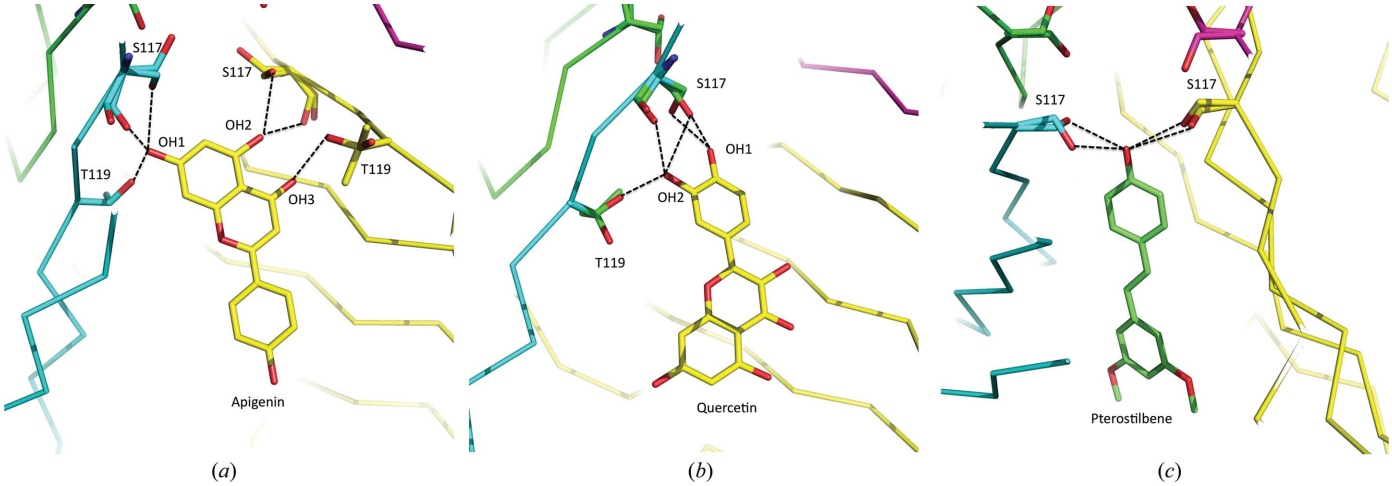

Figure 3
Hydrogen-bond interactions established by apigenin (*a*), quercetin (*b*) and petrostilbene (*c*) with protein atoms of residues lining the binding cavity are shown, along with portions of the C^{α} chain traces of chains *B* (cyan) and *B*′ (yellow).

Table 2
Distances between the C^{α} atoms of two equivalent pairs of residues in chains *A* and *B* for unliganded TTR and TTR–ligand complexes determined at a resolution of better than 1.4 Å.

PDB code	TTR complex	Thr40 distance (Å)	Lys70 distance (Å)
4mas	3,3′,5,5′-Tetrachloro-(1,1′-biphenyl)-4,4′-diol	11.83	15.10
3imt	(*E*)-4-(4-Aminostyryl)-2,6-dibromophenol	11.69	14.88
3p3r	(3,4-Dihydroxy-5-nitrophenyl)-(2-fluorophenyl)methanone	11.57	14.96
4hju	(*E*)-*N*-[3-(4-Hydroxy-3,5-dimethylstyryl)phenyl]acrylamide	11.45	14.82
Pterostilbene†	Pterostilbene	11.42	14.22
2qgb	Unliganded	11.40	14.82
2qge	2-(3,5-Dimethylphenyl)benzoxazole	11.38	14.86
1f41	Unliganded	11.17	14.61
4ky2	(*E*)-7-Hydroxy-3-(4-hydroxy-3,5-dimethylstyryl)-4-methyl-2*H*-chromen-2-one	10.99	14.54
Quercetin†	Quercetin	10.95	14.41
Apigenin†	Apigenin	10.94	14.50
4hjs	(*E*)-*N*-[4-(4-Hydroxy-3,5-dimethylstyryl]ethanesulfonamide	10.89	14.35
4l1t	(*E*)-3-(Dimethylamino)-5-(4-hydroxy-3,5-dimethylstyryl)benzoic acid	10.74	14.32
Tafamidis†	Tafamidis	10.40	14.22

† Data from this work.

Ser117 in monomers *B*′ and *B* (distances of 2.75 and 2.88 Å, respectively) and to its carbonyl O atom in monomers *B*′ and *B* (distances of 2.75 and 3.39 Å). One of these hydroxyls is also at 2.86 Å from the O^{γ} atom of Thr119 of monomer *B*′ (Fig. 3*a*; these interactions repeat themselves for the twofold axis-related ligand, with *B* and *B*′ reversed). In addition, the carbonyl O atom of the benzopyran ring is at a distance of 3.33 Å from the O^{γ} atom of Thr119, suggesting a very loose hydrogen-bond interaction. The remaining part of the ligand, in particular the phenyl ring, interacts with hydrophobic side chains of TTR, in particular Leu17, Ala108, Leu110 and Val121. On the contrary, the hydroxyl group bound to the phenyl ring does not specifically interact with protein atoms but is exposed to the external solvent.

3.1.2. TTR–quercetin complex. Distinctly from apigenin, in TTR-bound quercetin the benzopyran ring points towards the solvent and the dihydroxyphenyl ring points towards the inner part of the TTR cavity. In this case Ser117 is also involved in the ligand-binding stabilization, since its hydroxyl group can form a hydrogen bond to both of the hydroxyl groups of the phenyl ring of the ligand (OH1 to Ser117*B* O^{γ}, 2.49 or 2.29 Å; OH2 to Ser117*B* O^{γ}, 2.86 or 3.23 Å). OH2 is also at a distance of 3.03 Å from the hydroxyl group of Thr119 (Fig. 3*b*). One of the hydroxyl groups of the benzopyran ring also interacts with the O^{γ} atom of Thr119, whilst the other O atoms do not form any specific polar interactions.

3.1.3. TTR–pterostilbene complex. TTR-bound pterostilbene assumes a nearly planar conformation, with the phenol ring inside the cavity and the dimethoxyphenyl group pointing towards the solvent. The hydroxyl group points exactly towards the centre of the cavity, and in doing so can form a hydrogen bond to the O^{γ} atom of Ser117 of monomers *B* and *B*′ at the same time. Despite the double conformation of the latter residue, the distances are comparable (OH to Ser117*B* O^{γ}, 2.75 or 3.09 Å; OH to Ser117*B*′ O^{γ}', 2.64 or 3.03 Å; Fig. 3*c*). The bulk of the ligand interacts with the hydrophobic part of the cavity: Leu110, Leu17, Val121 and Ala108.

3.1.4. TTR–tafamidis complex. The structure of the complex of TTR with tafamidis has been reported previously (Bulawa *et al.*, 2012), but the data were measured again under the same experimental conditions as used for the other three complexes. The structure is identical to that deposited in the PDB and will not be described here, but the relevant feature is that both ligand sites are fully occupied by tafamidis.

3.2. Asymmetry of T4 binding sites

The most relevant feature of the structures of the TTR–ligand complexes described here is represented by the clear asymmetry of the two binding sites in the TTR molecule. In the crystal, the most significant differences among them are limited to the loop 98–103 and to the nearby C-terminus (residues 122–124). Flexibility of loop 98–103 has been observed in several other TTR structures deposited in the PDB: for example, in the crystal structure of uncomplexed TTR (PDB entry 1f41) determined at 1.5 Å resolution (Hörnberg *et al.*, 2000) this loop has two conformations. This different conformation can in turn induce a change in the position of the nearby C-terminal residues 122–124, which could affect ligand binding by slightly reducing the overall size of the cavity of site *B* relative to site *A*, and in particular the opening of the cavity. Despite this, the entrance to the cavity does not seem to play a major role in ligand binding, since in the crystal its size is smaller in site *B* than in site *A*, as opposed to the preferential binding of polyphenols to site *B*. The conformations of the side chains of the residues in the two cavities are also very similar, despite some minor differences that can affect the interaction with a potential ligand. In the TTR–pterostilbene complex the position of the C^{α} atom of Ser117 in monomer *A* increases the distance of the hypothetical position of the hydroxyl group of the ligand from the O^{γ} atom of Ser117 from 2.75 to 3.25 Å. In the case of quercetin the same effect induces an increase of the distances of OH1 and OH2 of the ligand from the O^{γ} atom of Ser117 from 2.30 to 2.65 Å and from 2.86 to 3.20 Å, respectively. For apigenin,

one of the hydrogen-bond distances decreases (from 2.88 to 2.43 Å) but all of the others increase, globally weakening the interaction. The effect of these variations results in some reduction in the strength of hydrogen-bond interactions (and possibly of other weak interactions), which can consequently lead to a reduction in the binding affinity for the second ligand. This could represent a general feature of the TTR sites, since the modifications introduced by the binding of one ligand can affect the network of hydrogen-bond interactions experienced by the second ligand, resulting in cooperativity in TTR binding. In very recent work based on a joint X-ray–neutron diffraction study (Haupt *et al.*, 2014), a significant role in the asymmetry of the binding sites was ascribed to Ser117.

Some asymmetry in the binding to the two TTR sites has previously been observed in the crystal structures of other TTR–ligand complexes (Palaninathan *et al.*, 2009; Tomar *et al.*, 2012), but this was limited to a weaker electron density in one of them. In the present case, the occupancy of one of the two binding sites is nearly negligible for two of the three TTR–ligand complexes and, notably, the empty site is always site *A*. In a previous study (Tomar *et al.*, 2012), the less occupied site in the crystal was indicated as site *B*, but a superposition with our structures shows that this is simply owing to a different labelling of the subunits. This indicates that the asymmetric binding of a ligand in the TTR tetramer is sufficient to direct the crystal growth in such a way that sites *A* and *B* are not equivalent in the crystal lattice. It should be pointed out that the TTR–ligand complexes considered in this study were prepared in solution and crystallized in order to avoid any influence of crystal packing in the formation of the complexes.

3.3. Molecular-dynamics and normal-mode calculations

In order to define the dynamics of the TTR tetramer in solution and the equivalence of the two binding sites,

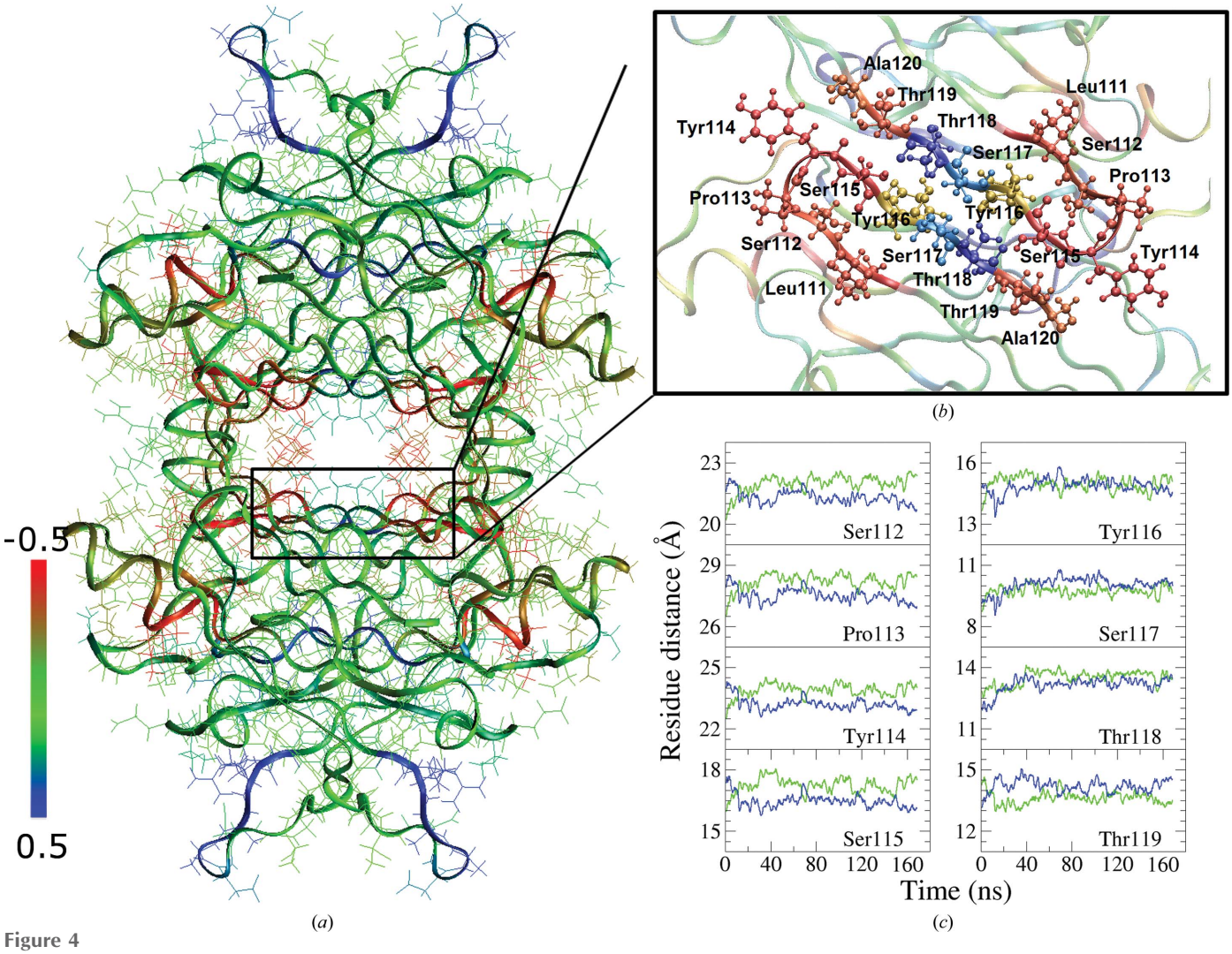

Figure 4
Distance correlations between equivalent C^{α} atoms in the *AA′* and *BB′* monomers during molecular dynamics. (*a*) shows a representation of the behaviour of the whole protein complex, while (*b*) shows details of the inner part of the tetramer. The colour code is from blue (distance changes are correlated) to red (distance changes are anticorrelated) through green (distances change are uncorrelated). The motion of residues 116–118 in the two dimers are correlated, while for all the other residues belonging to the inner cavity the distances are anticorrelated. (*c*) shows the variation of the distances of C^{α} atoms for selected residues belonging to the binding cavities during the simulation. The correlation (ρ) is computed for each pair of similar traces.

molecular-dynamics and normal-mode calculations have been performed. In particular, low-frequency relative motion of the four monomers of TTR can be revealed by normal modes. These were computed using the *elNémo* web server (Suhre & Sanejouand, 2004). The result of this calculation clearly indicated the existence of concerted fluctuations linked to the presence of four subunits in TTR. In particular, the second lowest frequency mode (Supplementary Fig. S1 and Supplementary Movie) clearly shows that as monomer *A* departs from monomer *A*′, monomer *B* become closer to monomer *B*′.

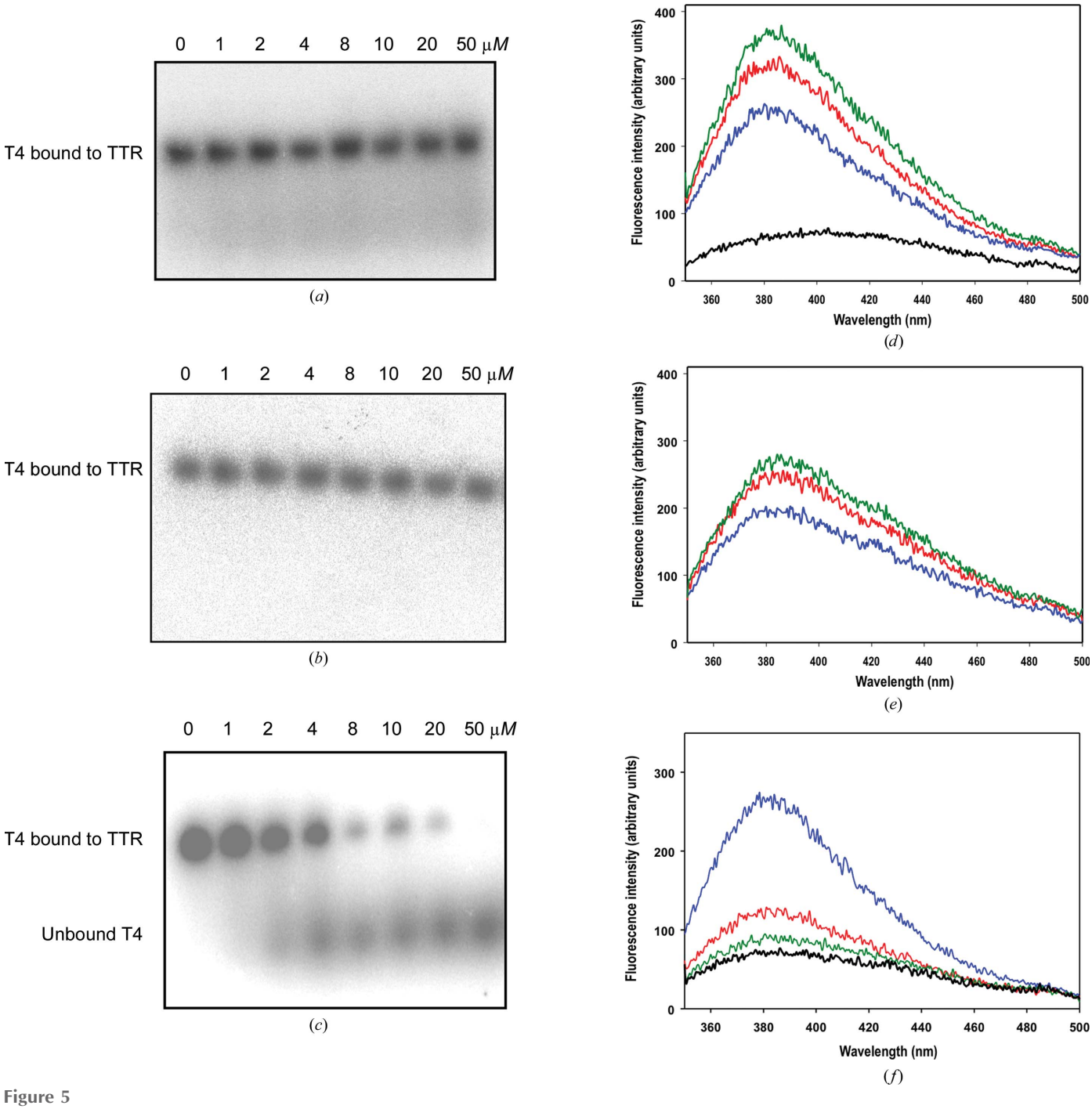

Figure 5
(*a*, *b*, *c*) Lack of displacement of TTR-bound radiolabelled T4 by pterostilbene and quercetin. Increasing concentrations (up to 50 μ*M*) of pterostilbene (*a*), quercetin (*b*) or cold T4 as a positive control (*c*) were added to 3 μ*M* TTR pre-incubated with a trace amount of radiolabelled T4 in PBS buffer. Radioactivity signals were recorded after nondenaturing PAGE. (*d*, *e*, *f*) Binding of pterostilbene to TTR and competition between pterostilbene, quercetin and T4. (*d*) Fluorescence emission spectra (excitation at 320 nm) of 2 μ*M* pterostilbene in the absence of TTR (black) and of 2 μ*M* (blue), 4 μ*M* (red) or 6 μ*M* (green) pterostilbene in the presence of 2 μ*M* TTR. (*e*) Fluorescence emission spectra (excitation at 320 nm) of 2 μ*M* (blue), 4 μ*M* (red) or 6 μ*M* (green) pterostilbene in the presence of 2 μ*M* TTR pre-incubated with 2 μ*M* cold T4. (*f*) Fluorescence emission spectra (excitation at 320 nm) of 2 μ*M* pterostilbene in the absence (black) and in the presence of 2 μ*M* TTR before (blue) and after the addition of 2 μ*M* (red) and 4 μ*M* (green) quercetin.

This movement takes place perpendicularly to the molecular twofold axis coincident with the long central cavity of TTR. This fluctuation is also confirmed to exist on shorter time scales by molecular-dynamics calculations, as summarized in Fig. 4 and in Supplementary Fig. S2. The analysis of trajectories shows that the distances between the positions of corresponding C^{α} atoms in the AA' and BB' subunits are correlated for a few residues in the centre of the TTR inner cavity, whilst they are anticorrelated for most of the other residues in the same cavity. Moreover, analysis of the atomic fluctuations (r.m.s.f.s) shows that the region around the TTR inner cavity is the most rigid, giving a further indication that the movement is concerted. Motions of residues far from the core of the tetramer appear to be uncorrelated. The most relevant result of this study is that following this fluctuation the two parts of the cavity become alternately larger and smaller, making the two binding sites not equivalent at a given instant. Similar results were also observed in previous shorter molecular-dynamics simulations (Wang *et al.*, 2007).

3.4. Competition binding assays

The experiments on the binding of pterostilbene or quercetin in the presence of radiolabelled ^{125}I-T4 as a competitor indicate that both compounds do not displace the TTR-bound hormone even at the highest concentrations tested (50 μM; Figs. 5*a*, 5*b* and 5*c*). Fluorescence data for pterostilbene indicate that this ligand binds to TTR both in the absence (Fig. 5*d*) and in the presence (Fig. 5*e*) of pre-incubated T4. Experiments on the binding of apigenin to TTR in the presence of radiolabelled ^{125}I-T4 as a competitor indicated that this ligand is able to displace the TTR-bound hormone only partially and at very high concentrations (Florio *et al.*, submitted). Moreover, owing to its higher binding affinity, at equimolar concentrations quercetin is able to induce the displacement of TTR-bound pterostilbene (Fig. 5*f*). Taken together, these data indicate that the three polyphenols bind to the same preferential site and that the hormone binds to a distinct preferential site in the TTR molecule.

4. Discussion

Hypotheses have been put forward to explain the molecular basis of the negative binding cooperativity of TTR (Reid *et al.*, 1989; Neumann *et al.*, 2001; Palaninathan *et al.*, 2009; Tomar *et al.*, 2012; Haupt *et al.*, 2014). In TTR, a crystallographic (and molecular) twofold axis runs along the two binding sites and two molecular twofold axes lie perpendicular to the crystallographic axis at the centre of the TTR tetramer. The molecular symmetry of TTR in solution is, in principle, 222, so that the four monomers should be indistinguishable; the labelling of sites *A* and *B* in TTR used in this and other work dealing with the structure of TTR assumes a meaning only in the crystal lattice, where intermolecular contacts render the monomers different. A consequence of the symmetry just described is not only that two ligands can be bound to the TTR tetramer at the same time, but also that in each of the two sites a non-symmetric molecule can bind in two different ways, each with half occupancy. This situation has often prevented a very detailed definition of the geometry of the molecule bound to TTR, despite the large number of structures of TTR–ligand complexes present in the PDB (Palaninathan, 2012). In this work, the relatively high resolution allows a clearer definition of the binding in comparison with previously deposited structures. The main point is that despite the fact that the two binding sites are identical in principle, only site *B* is fully occupied in all three of the TTR–ligand complexes that we have examined, whilst site *A* is nearly empty or only partially occupied. This situation is different from that found for several other TTR–ligand complexes for which structures have been determined at high resolution, as in the case of TTR-bound tafamidis (PDB entry 3tct; Bulawa *et al.*, 2012). Indeed, the electron-density map for the TTR–tafamidis complex prepared in our experimental conditions shows the presence of tafamidis in both binding sites and the occupancies of the ligand refined to the same value of 0.5 (Fig. 2*d*). A plausible explanation of our observation is that in the case of tafamidis the binding affinities of the two TTR sites ($K_{\rm diss}$ of $\sim$2 and $\sim$200 nM, respectively; Bulawa *et al.*, 2012), despite being different, are high enough to allow full saturation of both sites. Instead, the binding affinity of at least one of the two TTR sites for the three polyphenols considered in this study can be assumed to be significantly smaller than that of tafamidis for the same site, resulting in only negligible or partial saturation of the second binding site by the polyphenols examined under the same experimental conditions.

The question now arises as to whether these differences were already present in solution, since the crystals were grown from a complex prepared by incubating TTR in solution with the ligand. Molecular-dynamics simulations suggest that the two parts of the cavity undergo fluctuations, so that the two sites can be temporarily different, becoming alternatively larger and smaller with respect to the size observed in the crystal structure. If the simulation reflects the behaviour of TTR in solution, each ligand will enter the cavity that better fits it at a given moment in time, and in doing so affects the other cavity, eventually freezing it in a conformation that is less favourable for the binding of a second copy of the same ligand molecule.

If monomer *B* of a TTR–ligand complex is superimposed on monomer *B* of unliganded TTR, the position of monomer *A* is slightly displaced as a result of a very small rotation of about 1° (Supplementary Fig. S3). Since this reorientation is very small, it can be better appreciated by measuring the distance between two points far away from the centre of the tetramer. The distances between the C^{α} atoms of two pairs of such residues from monomers *A* and *B*, Thr40 and Lys70, are reported in Table 2 for our complexes and for other unliganded and complexed TTR structures present in the PDB and refined at high resolution. There is a relatively broad range of distances (10.74–11.83 Å for Thr40 and 14.22–15.10 Å for Lys70), corresponding to slightly different positions of one monomer relative to the other. Nevertheless, the longest and shortest distances correspond to the TTR structures with a

ligand bound inside the cavity, and the two unliganded TTR structures fall approximately in the middle of the range (Table 2). The flexibility that we observe in the crystal is much smaller in comparison with the movements predicted by molecular dynamics; nevertheless, it shows a tendency of the monomers to reorient with respect to each other in the tetramer. Binding data in solution clearly indicate the presence of an asymmetry of the two TTR binding sites, each of which shows preferential binding for distinct ligands, whilst in all the crystal structures of TTR–ligand complexes deposited in the PDB, including those presented in this work, the two sites are very similar and the small differences observed possibly do not justify the differences in binding observed in solution. The binding cooperativity effect in TTR is consistent with an allosteric behaviour of the tetramer according to molecular-dynamics simulations. The nature of this behaviour is of mechanical or, in other words, of a steric nature upon ligand binding. Ultimately, the rearrangement of hydrogen-bond patterns can be seen as a consequence of the variations of the intermolecular distances between monomers. Taking these observations together, it must be concluded that the packing forces in the crystal substantially reduce the flexibility of the tetramer, forcing the protein towards a more symmetric conformation during the crystallization process that does not reflect the flexibility present in solution.

5. Conclusions

The TTR–ligand complexes investigated in this study were prepared in solution, where the structure of uncomplexed TTR is not affected by the interaction of symmetry-related molecules present in the crystal lattice. We have unequivocally demonstrated that the two TTR binding sites can present significantly different occupancies. This behaviour is linked to a degree of plasticity and flexibility of the binding sites of the TTR tetramer, which deviates in solution transiently from a perfect 222 symmetry. In this way TTR is able to bind a large variety of small ligands of very different chemical nature and, through adjustments of the tetramer geometry, induces a binding cooperativity effect.

To date, the only drugs available for the therapy of TTR amyloidoses are tafamidis and diflunisal, which stabilize the native state of TTR (Adamski-Werner *et al.*, 2004; Bulawa *et al.*, 2012) and have proved to be effective in slowing neurological impairment in TTR amyloidosis (Obici & Merlini, 2014). Our results may have implications for the approach to new drug therapies for TTR amyloidosis. In fact, the asymmetry of the binding sites could be exploited for the development of a cocktail of two different compounds that takes advantage of this asymmetry. This might be performed in such a way that one drug has a higher affinity for the first binding site and the other drug, a different chemical compound, has a higher affinity for the second, altered, binding site.

Acknowledgements

We thank the staff of beamline PXIII at the Synchrotron Light Source (SLS), Villigen, Swtzerland for technical assistance during data collection. MC would like to thank Dr Thomas Schneider (EMBL Hamburg) for continuous support of this project. This work received financial support from the Universities of Padua and Parma, Italy, from MIUR (PRIN Project 2009KN2FBM), Rome, Italy and from the European Community's Seventh Framework Program (FP7/2007-2013) under grant agreement No 283570 (BioStruct-X).

References

Adams, P. D. *et al.* (2010). *Acta Cryst.* D**66**, 213–221.
Adamski-Werner, S. L., Palaninathan, S. K., Sacchettini, J. C. & Kelly, J. W. (2004). *J. Med. Chem.* **47**, 355–374.
Berendsen, H. J. C., Postma, J. P. M., van Gunsteren, W. F., DiNola, A. & Haak, J. R. (1984). *J. Chem. Phys.* **81**, 3684–3688.
Blake, C. C., Geisow, M. J., Oatley, S. J., Rérat, B. & Rérat, C. (1978). *J. Mol. Biol.* **121**, 339–356.
Bulawa, C. E., Connelly, S., Devit, M., Wang, L., Weigel, C., Fleming, J. A., Packman, J., Powers, E. T., Wiseman, R. L., Foss, T. R., Wilson, I. A., Kelly, J. W. & Labaudinière, R. (2012). *Proc. Natl Acad. Sci. USA*, **109**, 9629–9634.
Cendron, L., Trovato, A., Seno, F., Folli, C., Alfieri, B., Zanotti, G. & Berni, R. (2009). *J. Biol. Chem.* **284**, 25832–25841.
Cheng, S.-Y., Pages, R. A., Saroff, H. A., Edelhoch, H. & Robbins, J. (1977). *Biochemistry*, **16**, 3707–3713.
Choi, S., Reixach, N., Connelly, S., Johnson, S. M., Wilson, I. A. & Kelly, J. W. (2010). *J. Am. Chem. Soc.* **132**, 1359–1370.
Coelho, T., Maia, L. F., da Silva, A. M., Cruz, M. W., Planté-Bordeneuve, V., Suhr, O. B., Conceiçao, I., Schmidt, H. H.-J., Trigo, P., Kelly, J. W., Labaudinière, R., Chan, J., Packman, J. & Grogan, D. R. (2013). *J. Neurol.* **260**, 2802–2814.
Connelly, S., Choi, S., Johnson, S. M., Kelly, J. W. & Wilson, I. A. (2010). *Curr. Opin. Struct. Biol.* **20**, 54–62.
Darden, T., York, D. & Pedersen, L. (1993). *J. Chem. Phys.* **98**, 10089–10092.
Duan, Y., Wu, C., Chowdhury, S., Lee, M. C., Xiong, G., Zhang, W., Yang, R., Cieplak, P., Luo, R., Lee, T., Caldwell, J., Wang, J. & Kollman, P. (2003). *J. Comput. Chem.* **24**, 1999–2012.
Emsley, P. & Cowtan, K. (2004). *Acta Cryst.* D**60**, 2126–2132.
Evans, P. (2006). *Acta Cryst.* D**62**, 72–82.
Ferguson, R. N., Edelhoch, H., Saroff, H. A., Robbins, J. & Cahnmann, H. J. (1975). *Biochemistry*, **14**, 282–289.
Green, N. S., Foss, T. R. & Kelly, J. W. (2005). *Proc. Natl Acad. Sci. USA*, **102**, 14545–14550.
Haupt, M., Blakeley, M. P., Fisher, S. J., Mason, S. A., Cooper, J. B., Mitchell, E. P. & Forsyth, V. T. (2014). *IUCrJ*, **1**, 429–438.
Hörnberg, A., Eneqvist, T., Olofsson, A., Lundgren, E. & Sauer-Eriksson, A. E. (2000). *J. Mol. Biol.* **302**, 649–669.
Hurshman Babbes, A. R., Powers, E. T. & Kelly, J. W. (2008). *Biochemistry*, **47**, 6969–6984.
Johnson, S. M., Connelly, S., Fearns, C., Powers, E. T. & Kelly, J. W. (2012). *J. Mol. Biol.* **421**, 185–203.
Johnson, S. M., Wiseman, R. L., Sekijima, Y., Green, N. S., Adamski-Werner, S. L. & Kelly, J. W. (2005). *Acc. Chem. Res.* **38**, 911–921.
Kabsch, W. (2010). *Acta Cryst.* D**66**, 125–132.
Klabunde, T., Petrassi, H. M., Oza, V. B., Raman, P., Kelly, J. W. & Sacchettini, J. C. (2000). *Nature Struct. Mol. Biol.* **7**, 312–321.
Kolstoe, S. E. & Wood, S. P. (2010). *Biochem. Soc. Trans.* **38**, 466–470.
Monaco, H. L., Rizzi, M. & Coda, A. (1995). *Science*, **268**, 1039–1041.
Neumann, P., Cody, V. & Wojtczak, A. (2001). *Acta Biochim. Pol.* **48**, 867–875.
Obici, L. & Merlini, G. (2014). *Expert Opin. Investig. Drugs*, **23**, 1239–1251.
Painter, J. & Merritt, E. A. (2006). *Acta Cryst.* D**62**, 439–450.
Palaninathan, S. K. (2012). *Curr. Med. Chem.* **19**, 2324–2342.

Palaninathan, S. K., Mohamedmohaideen, N. N., Orlandini, E., Ortore, G., Nencetti, S., Lapucci, A., Rossello, A., Freundlich, J. S. & Sacchettini, J. C. (2009). *PLoS One*, **4**, e6290.
Pasquato, N., Berni, R., Folli, C., Alfieri, B., Cendron, L. & Zanotti, G. (2007). *J. Mol. Biol.* **366**, 711–719.
Pronk, S., Páll, S., Schulz, R., Larsson, P., Bjelkmar, P., Apostolov, R., Shirts, M. R., Smith, J. C., Kasson, P. M., van der Spoel, D., Hess, B. & Lindahl, E. (2013). *Bioinformatics*, **29**, 845–854.
Reid, D. G., MacLachlan, L. K., Voyle, M. & Leeson, P. D. (1989). *J. Biol. Chem.* **264**, 2013–2023.
Suhre, K. & Sanejouand, Y.-H. (2004). *Nucleic Acids Res.* **32**, W610–W614.
Tomar, D., Khan, T., Singh, R. R., Mishra, S., Gupta, S., Surolia, A. & Salunke, D. M. (2012). *PLoS One*, **7**, e43522.
Trivella, D. B. B., Bleicher, L., Palmieri, L. de C., Wiggers, H. J., Montanari, C. A., Kelly, J. W., Lima, L. M. T. R., Foguel, D. & Polikarpov, I. (2010). *J. Struct. Biol.* **170**, 522–531.
Trivella, D. B. B., dos Reis, C. V., Lima, L. M. T. R., Foguel, D. & Polikarpov, I. (2012). *J. Struct. Biol.* **180**, 143–153.
Wang, H., Tang, Y. & Lei, M. (2007). *Arch. Biochem. Biophys.* **466**, 85–97.
Weiss, M. S. (2001). *J. Appl. Cryst.* **34**, 130–135.
Westermark, P., Sletten, K., Johansson, B. & Cornwell, G. G. (1990). *Proc. Natl Acad. Sci. USA*, **87**, 2843–2845.
Winn, M. D. *et al.* (2011). *Acta Cryst.* D**67**, 235–242.
Wojtczak, A., Cody, V., Luft, J. R. & Pangborn, W. (1996). *Acta Cryst.* D**52**, 758–765.
Wojtczak, A., Neumann, P. & Cody, V. (2001). *Acta Cryst.* D**57**, 957–967.
Zanotti, G., Cendron, L., Folli, C., Florio, P., Imbimbo, B. P. & Berni, R. (2013). *FEBS Lett.* **587**, 2325–2331.
Zonta, F., Girotto, G., Buratto, D., Crispino, G., Morgan, A., Abdulhadi, K., Alkowari, M., Badii, R., Gasparini, P. & Mammano, F. (2015). *Hum. Mol. Genet.* **24**, 2641–2648.